Available online at www.sciencedirect.com

ScienceDirect

Procedia IUTAM 14 (2015) 536 – 542

Procedia IUTAM

www.elsevier.com/locate/procedia

IUTAM_ABCM Symposium on Laminar Turbulent Transition

The influence of stratification and slope in mixing layers

Taira, D. E.[a,*], Schettini, E. B. C.[b], Silvestrini, J. H.[c]

[a]*Instituto Federal Sul-rio-grandense (IFSul), Praça vinte de setembro, 455, Pelotas-RS, 96015-360, Brazil*
[b]*Instituto de Pesquisas Hidráulicas, Universidade Federal do Rio Grande do Sul (UFRGS), Av. Bento Gonçalves, 9500, Porto Alegre-RS, 91501-970, Brazil*
[c]*Faculdade de Engenharia, Pontifícia Universidade Católica do Rio Grande do Sul (PUCRS). Av. Ipiranga, 6681, Porto Alegre-RS, 90619-900, Brazil*

Abstract

The purpose of this numerical work is focused on the dynamics of a stably stratified inclined mixing layer. Both effects, stratification and slope, are considered through relevant flow parameters. Chebyshev's approximations and Direct Numerical Simulation (DNS) are used in the context of linear stability analysis for different Richardson numbers and slopes. Two-dimensional temporal and spatial simulations are employed to examine baroclinic layer and the evolution of primary and secondary Kelvin-Helmholtz instabilities. In three-dimensional configuration, only stratification effects are considered. The numerical results show persistence of the translative instability with formation of intense longitudinal vortices highly influenced by the Richardson number.

Selection and peer-review under responsibility of ABCM (Brazilian Society of Mechanical Sciences and Engineering)
Keywords: inclined mixing layer; stable stratification; Direct Numerical Simulation; linear stability analysis.

1. Introduction

Stratified mixing layers develop in the interface of two parallel streams of fluid moving with different velocities and densities. This kind of flows is often found in nature, such as in the atmosphere due to interaction among air currents or in the mixing between fresh and salt water. The buoyancy effect reduces the perturbation growth rate while the slope effect, for instance, due to topographical features, accelerates the developing of instabilities. The competition between both mechanisms results in various types of instabilities depending on mixing layer density difference and inclination. Thus, the transition to turbulence is governed by the competition between inertial and buoyancy forces, which strongly affect the mixing layer longitudinal spreading growth. Previous results of this kind of flows were obtained through laboratory experiments (Browand & Latigo[1] 1979, Thorpe[15] 1987), using linear stability analysis (Hazel[3] 1972, Negretti et al.[10] 2008), or by numerical simulations (Staquet[14] 2001, Smyth[12] 2003, Martinez et al.[9] 2007), among others.

The main objective of this numerical work is to study the stratification and slope influence in stably stratified mixing layers. Direct numerical simulation (DNS) and Chebyshev's approximations are used to quantify the temporal

* Corresponding author. Tel.: +55-53-2123-1020.
E-mail address: davi@pelotas.ifsul.edu.br

Selection and peer-review under responsibility of ABCM (Brazilian Society of Mechanical Sciences and Engineering)
doi:10.1016/j.piutam.2015.03.084

amplification of perturbations of linear problems. For spatially-developing simulations, 2D and 3D configuration domains are considered to follow the spatial evolution of primary and secondary instabilities and three-dimensional vortex structures.

2. Governing equations

The fluid motion governing equations are: continuity, Navier-Stokes in the Boussinesq approximation, and mass transport. In dimensionless, they are stated as,

$$\vec{\nabla}\cdot\vec{u}=0, \qquad \frac{\partial\vec{u}}{\partial t}+\frac{1}{2}[\vec{\nabla}(\vec{u}\otimes\vec{u})+(\vec{u}\cdot\vec{\nabla})\vec{u}]=-\vec{\nabla}\Pi+\frac{1}{Re}\vec{\nabla}^2\vec{u}+Ri\,\rho\,\vec{e_\theta}, \qquad \frac{\partial\rho}{\partial t}+(\vec{u}\cdot\vec{\nabla})\,\rho=\frac{1}{RePr}\nabla^2\rho, \tag{1}$$

where $\vec{u}=(u,v,w)$ is the velocity field, $\vec{e_\theta}=(sin\ \theta,\ -cos\ \theta,\ 0)$ with the slope given by θ (Fig. 1a), Π is the modified pressure field, and ρ the density. The reference parameters are half velocity difference ($U=(U_1-U_2)/2$), initial vorticity thickness ($\delta_i=2U/|\partial\overline{u}/\partial y|_{t=0,y=0}$) and density reference (ρ_0). The Reynolds number, bulk Richardson number and Prandtl number are defined, respectively, by $Re=U\delta_i/\nu$, $Ri=g\Delta\rho\delta_i/(2\rho_0U^2)$ and $Pr=\nu/\kappa$, where g is the gravitational acceleration, $\Delta\rho$ the density difference, ν the kinematic viscosity and κ the molecular diffusivity.

To perform linear stability analysis, the normal modes method is employed. The non-dimensional governing linear stability equation is given by

$$(\phi_{yy}-\alpha^2\phi)-\frac{u_{yy}}{(u-c)}\phi-Ri\,\frac{\rho_y\,cos\,\theta}{(u-c)^2}\phi-Ri\frac{sin\,\theta}{j\alpha(u-c)^2}\left[\rho_{yy}\phi-\frac{\rho_y u_y}{u-c}\phi+\rho_y\phi_y\right]=0, \tag{2}$$

where $u(y),\rho(y)$ are the base velocity and density profiles, subscripts y and yy denote differentiation with respect to the vertical direction, respectively, ϕ is the complex disturbance amplitude, $\alpha=\alpha_r$ is the wave-number, $c=\omega/\alpha=c_r+jc_i$ is the complex wave speed, and the amplification rate is defined by $\omega_i=\alpha_r c_i$. Density diffusion and viscous term have been neglected for Eq. (2) development.

3. Initial and boundary conditions

The velocity and density base profiles are given by

$$u(x,y,z,t)=U_C-U\,tanh\left(\frac{2y}{\delta_i}\right), \qquad v(x,y,z,t)=w(x,y,z,t)=0, \qquad \rho(x,y,z,t)=-\,tanh\left(\frac{2y}{\delta_\rho}\right), \tag{3}$$

where δ_ρ represents the initial density thickness and x, y and z are the streamwise, vertical and spanwise directions, respectively. For temporal simulations, the convection velocity is $U_C=0$ and initial conditions are $u=u(x,y,t=0)$, $\rho=\rho(x,y,t=0)$. Sinusoidal perturbation field (u_0',v_0') of maximum amplitude A_f is added to the base velocity profile. Boundary conditions are periodic at $x=0$ and $x=L_x$, and free-slip at $y=\pm L_y/2$. For spatially-developing mixing layers, the boundary conditions are $u=u(x=0,y,z,t)$, $\rho=\rho(x=0,y,z,t)$, $U_1=3U$, $U_2=U$ and $U_C=(U_1+U_2)/2$ (Fig. 1a). In the inflow boundary condition, the velocity and density profiles (Eq. 3) are used while at the outlet, an outflow boundary condition, $\frac{\partial\varphi}{\partial t}+U_C\frac{\partial\varphi}{\partial x}=0$ is solved where φ represents u,v or ρ.

4. Numerical methods

The governing equations (Eq. 1) are solved numerically using the `Incompact3d` computational code[5], which is based on compact sixth-order finite difference schemes for spatial differentiation and a second-order Adams-Bashforth scheme for time integration. To treat the incompressibility condition, a fractional step method requires to solve a Poisson equation. This equation is fully solved in spectral space via the use of relevant Fast Fourier Transforms. For three-dimensional simulations, a parallel version of the computational code based on a powerful 2D domain decomposition method is used[6]. The linear stability equation, Eq. (2), is solved via Chebyshev's approximations.

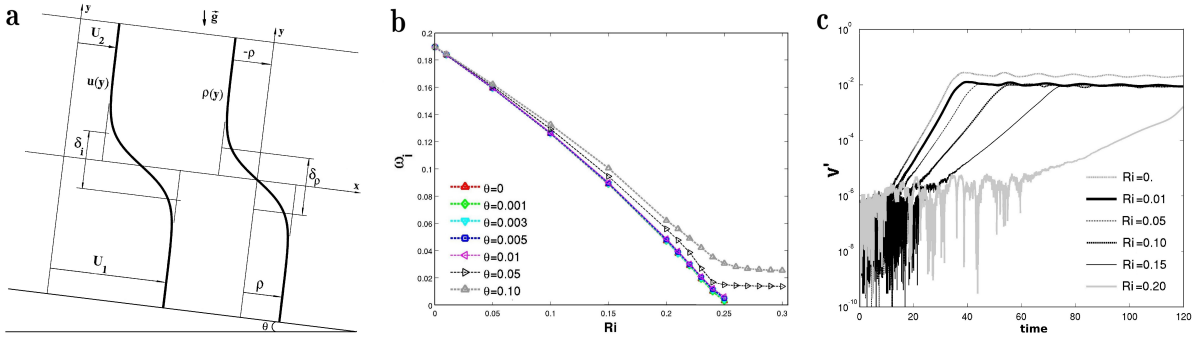

Fig. 1. (a) Mixing layer velocity and density base profiles; (b) Maximum amplification rate (Chebyshev operator); (c) Vertical disturbance temporal evolution for different Ri (grid (128, 129), $\theta = 0$).

5. Results

This section presents results regarding linear stability analysis and spatially-developing simulations focusing on stratification and slope influences in the mixing layer. Linear stability analysis using Chebyshev differential operator and *DNS* results are performed and compared.

5.1. Linear analysis

From Eq. (2), a third-order polynomial eigenvalue problem is obtained, where c is the eigenvalue. This problem is then transformed into a generalized eigenvalue problem[16,17]. This conversion is characterized by matrices of size $3N \times 3N$ where N is the total number of grid points. The bulk Richardson number used in analysis for linear stability lies between $0 \leq Ri \leq 0.30$ while the slope varies $0 \leq \theta \leq 0.10$. In Fig. 1b, for $\theta = 0$, the maximum growth rates present 10^{-4} order differences when compared with Hazel results[3] . For $0.001 \leq \theta \leq 0.01$, growth rates are undistinguished to the case for $\theta = 0$. When $\theta = 0.05$ and $\theta = 0.10$, the rates decrease as Ri increases but they remain above in comparison with the previous case and nearly constant for the highest Richardson numbers ($0.25 \leq Ri \leq 0.30$).

For two-dimensional temporal simulations, a $L_x = L_y = \lambda_a = 7\delta_i$ domain configuration is defined, which corresponds to the most amplified wavelength λ_a predicted by linear theory[3]. The dimensionless parameters are $Re = 300$, $Pr = 1$, $0 \leq Ri \leq 0.20$, $0 \leq \theta \leq 0.10$ and $A_f = 10^{-6}$. The largest mesh used is $(n_x, n_y) = (256, 257)$. The linear region for the vertical perturbation time evolution v', represents the maximum amplification (ω_i). When $\theta = 0$ (Fig. 1c), the numerical results obtained present a maximum difference of 0.21% when compared with the Chebyshev operator approach for the non-stratified case. When $0 < Ri \leq 0.10$, the error was less than 0.40% and reached up to 7.2% for the high stratification ($Ri = 0.2$).

Including stratification and slope effects, the maximum difference obtained between DNS and Chebyshev operator results is 1.25% for $Ri = 0.01$ and $\theta = 0.01$, increasing up to 2.12% when $Ri = 0.01$ and $\theta = 0.05$.

5.2. Spatial Simulations

For spatially-developing simulations, the following flow parameters are defined: $Re = 1000$, $Pr = 1$, and maximum perturbation amplitude $A_f = 0.10$. For two-dimensional simulations, the Richardson number ranges $0 \leq Ri \leq 0.10$, while for $Ri = 0.05$ the slope varies $0 \leq \theta \leq 0.10$. For three-dimensional simulations, only Ri number variation (with the same range) is considered. Table 1 summarizes flow and domain parameters for spatial simulations. The mesh grid is stretched in y, where the minimal mesh size is $\Delta y_{min} \cong 0.064\delta_i$ in $y \cong 0$. The simulation time is $320\delta_i/U$ which is equivalent to ≈ 45 Kelvin-Helmholtz (KH) vortices' emissions.

The evolution of the KH instability in a stably stratified mixing layer is firstly analysed through 2D simulations. The stratification level interferes in the flow dynamics, specifically, the baroclinic layer generation is intensified when the Ri number increases. In Figure 2, vorticity fields for $Ri = 0$ (Fig. 2a), $Ri = 0.025$ (Fig. 2b), $Ri = 0.05$ (Fig. 2c) and

Table 1. Parameters for spatial simulations.

2*D* Simulation	*Ri*	θ	A_f	(L_x, L_y)	(n_x, n_y)	$\Delta t(\times 10^{-3})$
I	0	0	0.06	(147, 35)	(2497, 545)	2.5
II	0.025	0	0.06	(168, 28)	(2801, 521)	3
III	0.05	0	0.06	(168, 28)	(2881, 541)	2.5
IV	0.05	0.02	0.06	(168, 28)	(2881, 541)	2.5
V	0.05	0.05	0.06	(168, 28)	(3201, 577)	2
VI	0.05	0.10	0.06	(168, 28)	(3201, 673)	1.5
VII	0.10	0	0.10	(168, 28)	(3201, 673)	1.5
3*D* Simulation	*Ri*	θ	A_f	(L_x, L_y, L_z)	(n_x, n_y, n_z)	$\Delta t(\times 10^{-3})$
VIII – XII	0; 0.025; 0.05; 0.07; 0.1	0	0.12	(140, 49, 14)	(1417, 505, 72)	4

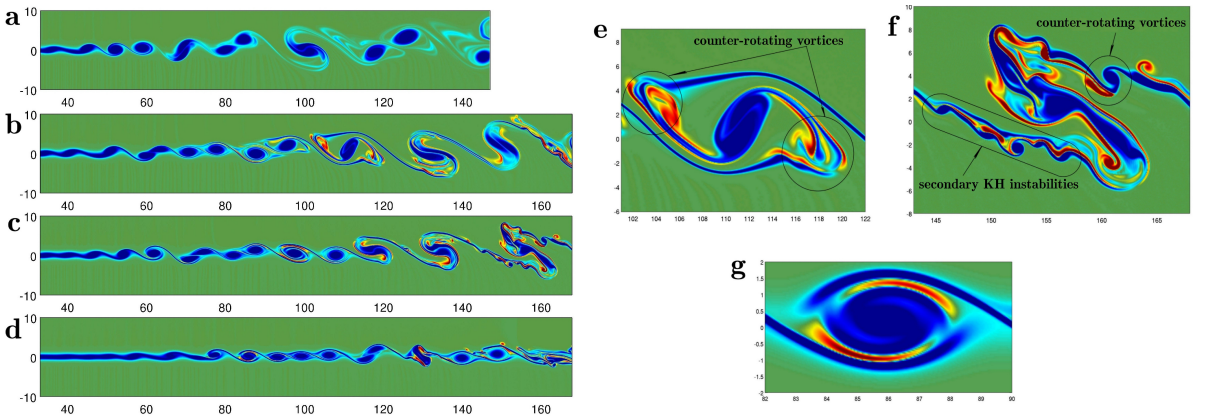

Fig. 2. Spanwise vorticity fields (ω_z) for: (a) $Ri = 0$; (b) $Ri = 0.025$; (c) $Ri = 0.05$; (d) $Ri = 0.10$. Spanwise vorticity fields: (e) in $x = 110$ for $Ri = 0.025$; (f) in $x = 155$ for $Ri = 0.05$; (g) in $x = 86$ for $Ri = 0.10$. Scale values ranging from -1.2 (blue) to 1.2 (red).

$Ri = 0.10$ (Fig. 2d) are shown. In the homogeneous mixing layer, after pairing, the KH vortex saturates since there is no source of energy for generating other instabilities. In a stratified flow, the vorticity layers are strained in between the KH vortices and form the baroclinic layer ($x \cong 125$ in Fig. 2b and c)[13]. The longitudinal density gradient ($\partial\rho/\partial x$) intensifies the baroclinic layer while reinforcing the vorticity layer and decreasing it in the vortex core. Therefore, the source term $\partial\rho/\partial x$ contributes with an additional mechanism for vorticity generation in the two-dimensional stratified layer[8].

For $Ri = 0.025$ (Fig. 2b), the baroclinic layer weakens due to emergence of a sub-harmonic instability and strengthens after the first pairing. The instability next to the core propagates towards the baroclinic layer, providing the appearance of counter-rotating vortices pairs (in red color and highlighted with a circle in Fig. 2e). This mechanism generates KH vortices in the baroclinic layer through a secondary instability that destabilizes the baroclinic layer. Secondary KH vortices are shown in Fig. 2b, centered at $x = 160$. The core instability is intensified for high stratification, for instance, when the Richardson number is $Ri = 0.05$ (Fig. 2c) and $Ri = 0.10$ (Fig. 2d). In these cases, the secondary KH instability mechanism can be noticed when $x \geq 130$ in Fig. 2c and $x \geq 140$ in Fig. 2d. Figure 2f shows a spanwise vorticity field of a zoomed in area of Fig. 2c centered at $x = 155$, confirming secondary *KH* instability and counter-rotating vortices. For the high stratified mixing layer case corresponding to $Ri = 0.10$ (Fig. 2d), the secondary KH vortices evolvement is inhibited due to the strong stratification that prevents the growth of the sub-harmonic mode. The core instability (Fig. 2g, $x = 86$) occurs before the pairing, as verified by temporal simulation of Martinez[7] (2006) and Staquet[13](1995) for $Re = 1000$ and $Ri = 0.083$.

The spatial evolution of the vorticity thickness δ_ω is now considered for quantifying the stratification influence on the mixing layer lateral spreading growth. In Fig. 3a, it can be observed how the vorticity thickness is strongly influenced by the Richardson number, decreasing its growing for increasing *Ri*. Figure 3b shows the spreading rate $(1/R)d\delta_\omega/dx$ as a function of the Richardson number for region $40 \leq x \leq L_x$, where the modified velocity ratio is

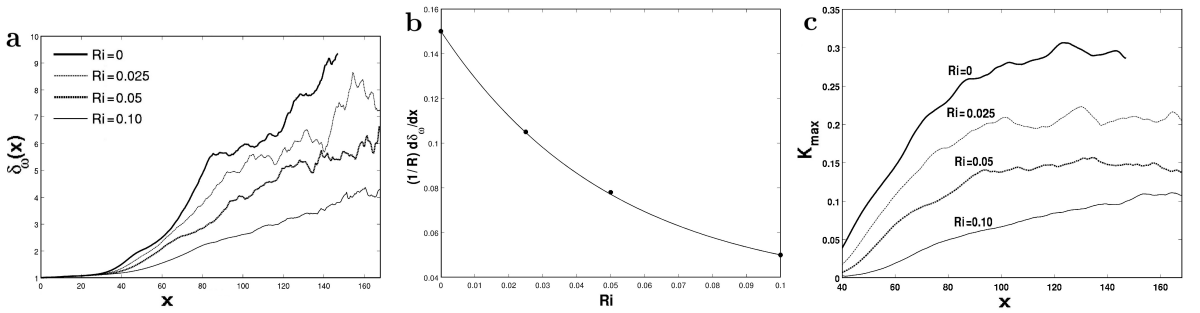

Fig. 3. (a) Spatial evolution of the vorticity thickness for 2D simulations; (b) Spreading rate (•) of the vorticity thickness as a function of the Richardson number and the adjusted function (−); (c) Spatial evolution of the maximum kinetic energy for $0 \leq Ri \leq 0.10$.

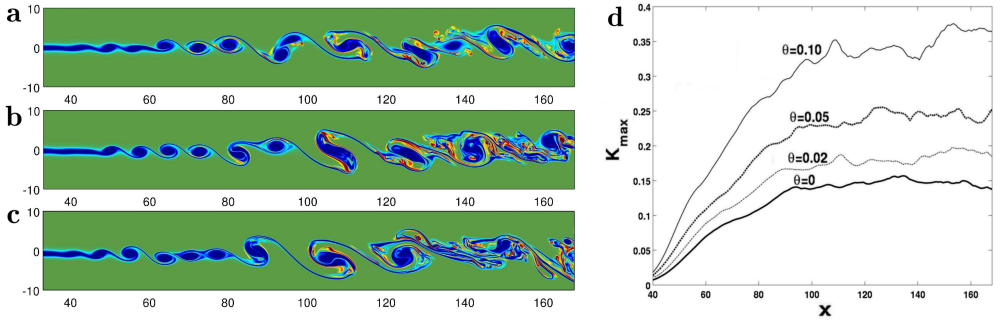

Fig. 4. Spanwise vorticity fields (ω_z) for $Ri = 0.05$ and: (a) $\theta = 0.02$; (b) $\theta = 0.05$; (c) $\theta = 0.10$; (d) Maximum kinetic energy streamwise evolution for $Ri = 0.05$ and $\theta = 0; 0.02; 0.05; 0.10$. Scale values ranging from −1.2 (blue) to 1.2 (red).

$R = (U_1 - U_2)/(U_1 + U_2) = 1/2$. This rate, defined by Brown & Roshko[2](1974) for homogeneous mixing layers, is extended here for the stratified case. Browand & Latigo[1](1979) computed a spreading rate of 0.15 for $Ri = 0$. An exponential function is adjusted based on the results, yielding the expression $f(Ri) = 0.034 + 0.116 \times 10^{-8.6Ri}$ (Fig. 3b).

The turbulent kinetic energy is also strongly influenced by stratification (Fig. 3c). For each streamwise position x, the maximum kinetic energy (K_{max}) was computed, where K is given by $K(x, y) = 0.5(< u'^2 > + < v'^2 >)$. The damping effect over the kinetic energy when $Ri > 0$ occurs because the stratification weakens the vertical motions.

Results from simulations IV, V, and VI (see Table 1) are now considered to analyse changes in the streamwise development of a stratified mixing layer ($Ri = 0.05$) when slope effects ($\theta = 0.02; 0.05; 0.1$) are taken into account. Comparing the results of simulation III ($\theta = 0$, Fig. 2c) and simulation IV ($\theta = 0.02$, Fig. 4a), it can be observed that there is an intensification of the secondary instability leading to a greater number of secondary KH vortices ($x \geq 120$) due to the increase slope. This effect is related with the horizontal forcing component $Ri\rho sin(\theta)$ in Eq.(1).

After the first pairing, the evolution of the KH vortices changes when a higher slope is considered (see, for instance, Fig. 4b for $\theta = 0.05$ and Fig. 4c for $\theta = 0.10$). The baroclinic layer formed between two adjacent pairings is more stretched with increasing slope, mainly when $\theta = 0.10$ (Fig. 4c). This can be interpreted by the source term $Ri[-(\partial\rho/\partial x)\cos\theta - (\partial\rho/\partial y)\sin\theta]$ that contributes as an additional mechanism for the vorticity generation in a two-dimensional stratified inclined mixing layer. The slope growth also influences the evolution of the maximum kinetic energy, K_{max} (Fig. 4d). The destabilizing effect produced by the component $Ri\,\rho\ sin(\theta)$ in Eq.(1) increases the kinetic energy. Therefore, higher levels of saturation are reached with increasing θ.

The three-dimensional behaviour of a spatially developing horizontal stratified mixing layer is considered now for $Ri = 0; 0.025; 0.05; 0.07; 0.1$ (Table 1). Fig. 5 shows instantaneous views of turbulent structures for different stratification levels (Table 1) through visualizations of Q-criterion. Pierrehumbert & Widnall[11](1982) investigated the formation of longitudinal vortices in a homogeneous mixing layer. The authors suggest that a translative instability

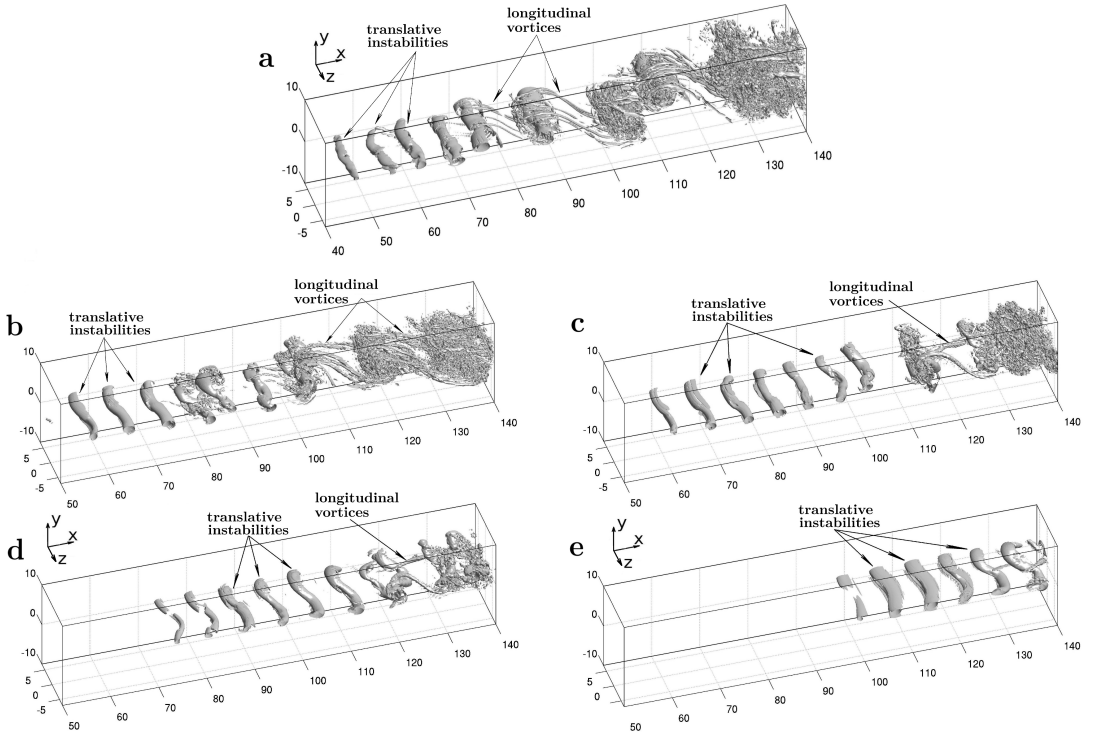

Fig. 5. Turbulent structures of a stratified mixing layer by iso-surfaces of Q-criterion with a iso-value $Q = 0.3$ for : (a) $Ri = 0$; (b) $Ri = 0.025$; (c) $Ri = 0.05$; (d) $Ri = 0.07$; and $Q = 0.2$ for (e) $Ri = 0.10$.

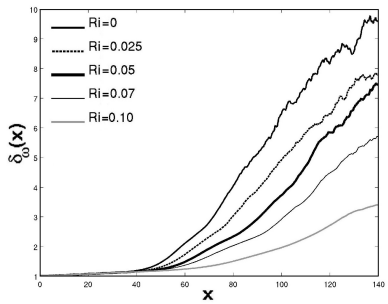

Fig. 6. Streamwise growing of the vorticity thickness for different Richardson numbers.

is responsible for the appearance of longitudinal vortices. Such instability is characterized by an in-phase spanwise oscillation of the KH vortex. The translative instability denoted indicated by arrows in Fig. 5 seems to be present in all stratified cases. As a result of this instability, strong longitudinal vortices are stretched between the KH big rollers in the homogeneous case (Fig. 5a). For increasing Ri numbers the streamwise structures seem to weaken due to stratification effect. Anyway they can be still observed even for $Ri = 0.1$, the highest stratification level here considered.

For the homogeneous case, the vorticity thickness spreading rate varies from 0.15 (Browand & Latigo[1]) to 0.27 (Huang & Ho[4]). For the stratified cases, this quantity was computed and its result is shown in Fig 6. A fair linear growth of the vorticity thickness appears to be expected with the higher influence for an increasing Ri number. The spatially growing vorticity thickness normalized with the velocity differences $(1/R)\delta_\omega/dx$ ranges from 0.201 ($Ri = 0$) to 0.062 ($Ri = 0.10$).

Conclusion

The purpose of this numerical study is to investigate stratification and slope influence in a stably stratified mixing layer. For the linear analysis, numerical solutions using Chebyshev operators and 2D simulations were performed. For stratified horizontal cases ($\theta = 0$), maximum growth rate differences of 10^{-4} were obtained when compared with the results using Chebyshev operators with reference[3]. For $\theta = 0.05$ and $\theta = 0.10$, the maximum growth rates decreased when Ri increases. Temporal simulations for $Re = 300$ show satisfactory results compared with Chebyshev operators for a wide range of Ri numbers and $\theta = 0.05$. Two-dimensional spatial developing simulations at $Re = 1000$ show vorticity layers strained in between the KH vortices forming a baroclinic layer. Depending on the Ri value, the baroclinic layer may develop secondary KH vortices. The streamwise evolution of the vorticity thickness is strongly influenced by the Richardson number, decreasing its lateral growth for increasing Ri. A potential law is proposed for the lateral spreading of the stratified mixing layer. The kinetic energy of the flow shows damping effects with increasing stratification. Results from three-dimensional spatially-developing stratified mixing layer simulations suggest that the translative instability is responsible for the appearance of longitudinal vortices. These streamwise vortices are stretched between the KH vortices for the homogeneous case. For increasing Ri, these structures are weakened due to stratification effect even though they can be still observed for the highest stratification considered here.

Acknowledgements

This research was performed with support from CNPq and the Centro Nacional de Supercomputação da Universidade Federal do Rio Grande do Sul (CESUP/UFRGS).

References

1. Browand FK., Latigo, B. *Growth of the two dimensional mixing layer from a turbulent and non-turbulent boundary layer*. Phys. Fluids, 1979; **22**: 1011-1019.
2. Brown GL., Roshko A. (1974) On density effects and large structure in turbulent mixing layers. J. Fluid Mech, 1974; **64**:775-816.
3. Hazel P. *Numerical studies of the stability of inviscid stratified shear flows*. J. Fluid Mech. 1972; **51**:39-61.
4. Huang L., Ho C. *Small-scale transition in a plane mixing layer*. J. Fluid Mech, 1990; **210**: 475-500.
5. Laizet S, Lamballais E. *High-order compact schemes for incompressible flows: A simple and efficient method with quasi-spectral accuracy*. J. Comp. Phys. 2009; **228**: 5989-6015.
6. Laizet S., Li N. *Incompact3d: A powerfull tool to tackle turbulence problems with up to O*(10^5) *computational cores*. Int. J. Numer. Methods Fluids, 2010; **67**: 1735-1757.
7. Martinez DMV. *Transição à Turbulência na camada de mistura estavelmente estratificada utilizando simulação numérica direta e simulação de grandes escalas*. PhD thesis, 2006. Universidade Federal do Rio Grande do Sul, Brasil, pp.1-152.
8. Martinez DMV., Schettini EBC., Silvestrini, JH. *Secondary Kelvin-Helmholtz instability in a 3D stably stratified temporal mixing layer by Direct Numerical Simulation*. Congresso sobre Métodos Numéricos y sus Aplicaciones. Santa Fé, 2006. Asociación Argentina de Mecánica Computacional, 1-13.
9. Martinez DMV., Schettini EBC., Silvestrini, JH. *The formation of streamwise vortics in a 3D stably stratified temporal mixing layer by Large-Eddy-Simulation*. 19th International Congress of Mechanical Engineering, 2007. Brasília, DF, Brazil.
10. Negretti ME., Socolofsky, SA., Jirka, GH. *Linear stability analysis of inclined two-layer stratified flows*. Physics of Fluids, 2008: **20**. doi:10.1063/1.2980351.
11. Pierrehumbert RT., Widnall SE. *The two and three-dimensional instabilities of a spatially periodic shear flows*. J. Fluid Mech., 1982; **114**: 59-82.
12. Smyth WD. *Secondary Kelvin-Helmholtz instability in weakly stratified shear flow*. J. Fluid Mech., 2003 **497**:67-98.
13. Staquet C. *Two-dimensional secondary instabilities in a strongly stratified shear layer*. J. Fluid Mech., 1995; **296**:73-126.
14. Staquet C., Bouruet-Aubertot P. *Mixing in weakly turbulent stably stratified flows*. Dynamics of Atmospheres and Oceans, 2001; **34**: 81-102.
15. Thorpe SA. *Transitional phenomena and the development of turbulence in stratified fluids: A review*. Journal of Geophysical Research, 1987; **92C**: 5231-5248.
16. Tisseur F. *Backward error and condition of polynomial eigenvalue problems*. Linear Algebra and its Applications. 2000; **309**: 339-361
17. Trefethen LN. *Spectral methods in MATLAB*. Philadelphia: SIAM, 2000, p. 145-152.